

High-pressure thermoelasticity of body-centered-cubic tantalum

O. Gülseren^{1,2,3} and R. E. Cohen³

¹*NIST Center for Neutron Research, National Institute of Standards and Technology, Gaithersburg, Maryland 20899*

²*Department of Materials Science and Engineering, University of Pennsylvania, Philadelphia, Pennsylvania 19104*

³*Geophysical Laboratory and Center for High Pressure Research, Carnegie Institution of Washington,*

5251 Broad Branch Road, NW, Washington, DC 20015

(Received 26 June 2001; published 3 January 2002)

We have investigated the thermoelasticity of body-centered-cubic (bcc) tantalum from first principles by using the linearized augmented plane wave and mixed-basis pseudopotential methods for pressures up to 400 GPa and temperatures up to 10 000 K. Electronic excitation contributions to the free energy were included from the band structures, and phonon contributions were included using the particle-in-a-cell (PIC) model. The computed elastic constants agree well with available ultrasonic and diamond-anvil cell data at low pressures, and shock data at high pressures. The shear modulus c_{44} and the anisotropy change behavior with increasing pressure around 150 GPa because of an electronic topological transition. We find that the main contribution of temperature to the elastic constants is from the thermal expansivity. The PIC model in conjunction with fast self-consistent techniques is shown to be a tractable approach to studying thermoelasticity.

DOI: 10.1103/PhysRevB.65.064103

PACS number(s): 62.20.Dc, 46.25.Hf, 62.20.-x, 71.20.Be

Single crystal elastic constants of solids at high pressures and temperatures are essential in order to predict and understand material response, strength, mechanical stability, and phase transitions. We have studied the high-pressure and temperature elastic constants of body-centered-cubic (bcc) tantalum, a group V transition metal, from first principles. Because of its high-structural mechanical, thermal, and chemical stability, Ta is a useful high-pressure standard.¹ Ta has a very high melting temperature 3269 K at ambient pressure. bcc Ta is stable to 174 GPa, according to diamond-anvil-cell experiments.¹ Shock compression experiments² show no transition other than melting (at around 300 GPa). Its stability makes Ta an ideal material for understanding the generic behavior of transition metals under compression, without the complication of phase transitions. Recently, its static properties were studied by full-potential LMTO calculations³ and the thermal equation of state was reported.⁴

The three elastic constants c_{11} , c_{12} , and c_{44} completely describe the elastic behavior of a cubic crystal. A more convenient set for computations are c_{44} and two linear combinations K and c_s . The bulk modulus

$$K = (c_{11} + 2c_{12})/3, \quad (1)$$

is the resistance to deformation by a uniform hydrostatic pressure; the shear constant

$$c_s = (c_{11} - c_{12})/2, \quad (2)$$

is the resistance to shear deformation across the (110) plane in the $[1\bar{1}0]$ direction, and c_{44} is the resistance to shear deformation across the (100) plane in the $[010]$ direction. The bulk modulus K was determined from the equation of state,⁴ using the Vinet equation.^{5,6} We obtained the shear moduli by straining the bcc lattice at fixed volumes using volume conserving tetragonal and orthorhombic strains for c_s and c_{44} , respectively, and computing the free energy as a function of strain. c_s was obtained by applying the following isochoric strain

$$\epsilon = \begin{pmatrix} \delta & 0 & 0 \\ 0 & \delta & 0 \\ 0 & 0 & (1 + \delta)^{-2} - 1 \end{pmatrix}, \quad (3)$$

where δ is the magnitude of the strain. Then the strain energy is

$$F(\delta) = F(0) + 6c_s V \delta^2 + O(\delta^3), \quad (4)$$

where $F(0)$ is the free energy of the unstrained system and V is its volume. Similarly, c_{44} was calculated from the following strain:

$$\epsilon = \begin{pmatrix} 0 & \delta & 0 \\ \delta & 0 & 0 \\ 0 & 0 & \delta^2/(1 - \delta^2) \end{pmatrix} \quad (5)$$

with the corresponding strain energy

$$F(\delta) = F(0) + 2c_{44} V \delta^2 + O(\delta^4). \quad (6)$$

The quadratic coefficients of strain energy gives the elastic constants. First order terms due to the initial stress (hydrostatic pressure)⁷ were eliminated by applying isochoric strains. Then, the elastic constants c_{11} and c_{12} were obtained from c_s and K .

We assume that the Helmholtz free energy of the system can be separated as⁸⁻¹⁰

$$F(V, T) = E_0(V) + F_{el}(V, T) + F_{vib}(V, T), \quad (7)$$

where $E_0(V)$ is the static zero temperature energy, $F_{el}(V, T)$ is the electronic contribution, and $F_{vib}(V, T)$ is the vibrational contribution to the free energy. Our computational procedure is based on density functional theory (DFT) generalized to finite temperatures by the Mermin theorem.¹¹ The charge density is temperature dependent through occupation numbers according to the Fermi-Dirac distribution, giving the electronic entropy from

$$S_{\text{el}} = \sum f_i \ln f_i + (1 - f_i) \ln(1 - f_i), \quad (8)$$

where $f_i = f_i(E - E_F, T)$ is the Fermi occupation at T for each state i . The variations of f_i with temperature were included from the self-consistent band structures calculated at an electronic temperature of 2000 K varying according to the Fermi-Dirac distribution.

The electronic excitations, both the static energy and the electronic contribution to the free energy, were computed by using the full potential linearized augmented plane wave (LAPW) method.^{12,13} The $5p$, $4f$, $5d$, and $6s$ states were treated as band states, and the deeper states were treated as soft core electrons. The generalized gradient approximation (GGA) (Ref. 14) was used for the exchange-correlation potential. The convergence of strain energies with respect to the Brillouin zone integration was carefully checked by repeating the calculations for $16 \times 16 \times 16$ and $24 \times 24 \times 24$ meshes at $V = 16.82 \text{ \AA}^3$ and we found at most 2 GPa (3%) difference both for c_s and c_{44} . Hence, we used $16 \times 16 \times 16$ special k -point meshes¹⁵ in the full Brillouin zone giving 344 and 612 k points within IBZ of tetragonal and orthorhombic lattice, respectively. The convergence parameter RK_{max} was 9 giving about 1800 plane waves and 200 basis functions per atom at zero pressure.

The vibrational free-energy was obtained within the particle-in-a-cell (PIC) model¹⁶ by using an accurate pseudopotential mixed-basis total energy method¹⁷ which is computationally more efficient than the LAPW calculations. In PIC, an atom is displaced in its Wigner-Seitz cell in the potential field of all the other atoms fixed at their equilibrium positions, i.e., the ideal, static lattice except for the wanderer atom. The partition function, and hence the free energy is calculated from this potential energy surface via an integral over the position of a single atom inside the Wigner-Seitz cell. The PIC model is essentially an anharmonic Einstein model, and the $3N$ -dimensional partition function is reduced to a simple three-dimensional (3D) integral.^{4,9} The advantage of the cell model over lattice dynamics based on the quasi-harmonic approximation is that anharmonic contributions from the potential-energy of the system have been included exactly without a perturbation expansion. On the other hand, since we used the classical partition function, and the interatomic correlations between the motions of different atoms is ignored, it is only valid at high temperatures above the Debye temperature (245 K in Ta).¹⁸ Since the vacancy formation energy is very high in Ta,¹⁹ spontaneous formation of defects is only important after the melting temperature.

For the PIC computations, a supercell with 54 atoms was used. The pseudopotential mixed-basis calculations were carried out on this 54 atoms supercell using LDA (Ref. 20) for exchange-correlations effects and $2 \times 2 \times 2$ k -point mesh resulting four special \vec{k} points for BZ integrations. A semirelativistic, nonlocal, and norm-conserving Troullier-Martins²¹ pseudopotential (with associated pseudo atomic orbitals) with nonlinear core corrections²² was used for the Ta atoms as described in detail in our previous study of thermal equation of state of Ta.⁴ After checking the energy convergence 550 and 60 eV are used as plane wave energy cutoffs for the

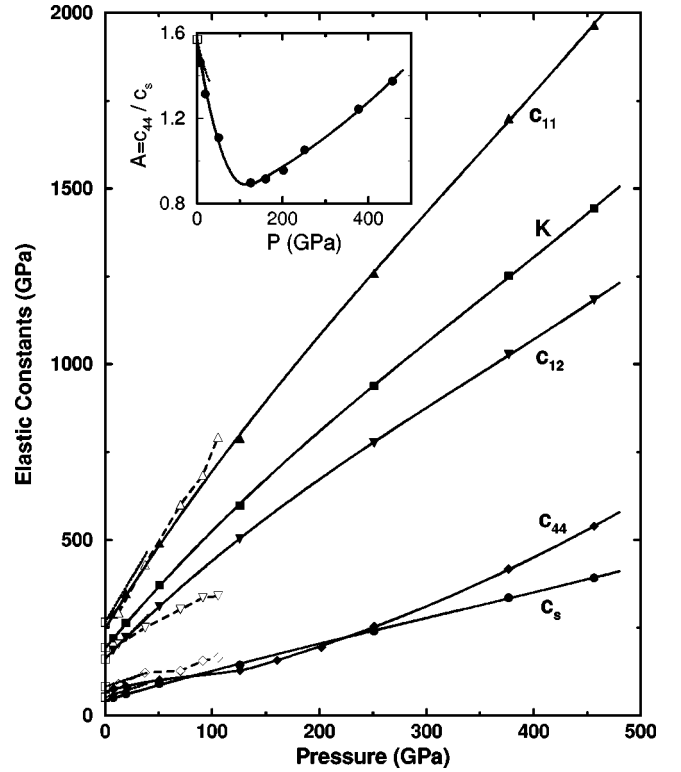


FIG. 1. Static elastic constants of Ta as a function of pressure. Open squares are ultrasonic experimental data of Katahara *et al.* (Refs. 24,25) and the dotted lines show the initial slopes. Open symbols are SAX data of Cynn and Yoo (Ref. 26). The anisotropy ratio is shown in the inset.

expansion of the pseudoatomic orbitals as well as FFT grid and low-energy plane waves for additional degrees of freedom in basis set, respectively. The canonical partition function was computed from the potential energy surface as a function of displacements of wanderer atom along special symmetry directions.^{9,23} We used 2 and 4 special directions for tetragonal and orthorhombic distortions, respectively, which integrates exactly up to $l=6$ lattice harmonics.²³ The potential energy was calculated at 4–6 different displacements along each of these special directions, and was fit to an even polynomial up to order six. Details of all the computational parameters were described previously.⁴

The static elastic constants as functions of pressure are presented in Fig. 1 and Table I. The zero pressure values and initial slopes are in good agreement with the ultrasonic experimental data of Katahara *et al.*^{24,25} Similarly, comparison with recent SAX (stress/angle-resolved x-ray diffraction) experimental data²⁶ up to 105 GPa shows good agreement for c_{11} and c_{44} . Likewise, c_{12} agrees well at low pressures, but deviates with increasing pressure. This may be due to the assumed isostress condition for experimental data analysis for all pressures, or due to the large uncertainty on measured deviatoric stress at high pressures. Note that, the initial slope of ultrasonic data agrees very well with our calculated c_{12} . The anisotropy ratio $A = c_{44}/c_s$ (inset Fig. 1) first decreases from 1.57 to 0.9 with increasing pressure, and then its slope reverses and it increases with increasing pressure. This is due to the changes in c_{44} . The change in behavior of c_{44} around

TABLE I. The static elastic constants for bcc tantalum. All elastic constants as well as pressure units are GPa.

$V(\text{\AA}^3)$	Pressure	K	c_{44}	c_s	c_{11}	c_{12}
18.39	-0.76	187.89	66.30	42.12	244.05	159.82
17.66	7.56	220.35	75.13	51.41	288.90	186.08
16.82	19.35	263.82	82.73	62.89	347.68	221.90
15.22	50.88	371.07	101.15	91.30	492.79	310.20
13.01	125.70	598.02	129.18	143.78	789.73	502.17
12.43	160.63	696.44	156.64			
11.67	202.01	808.93	194.45			
11.03	250.90	937.44	253.95	241.48	1259.41	776.46
9.83	376.54	1251.81	417.35	335.65	1699.34	1028.04
9.26	456.48	1443.14	538.35	391.79	1965.52	1181.94

150 GPa is due to the electronic transition evident in the equation of state.⁴ This indicates that elastic constants can be much more sensitive to changes in the Fermi surface than the equation of state, where the electronic transition was not apparent without examining small residuals in the equation of state fit.

The elastic constants of Ta as functions of temperature at various pressures are presented in Fig. 2 and Table II. In order to compare with experimental data, the computed iso-

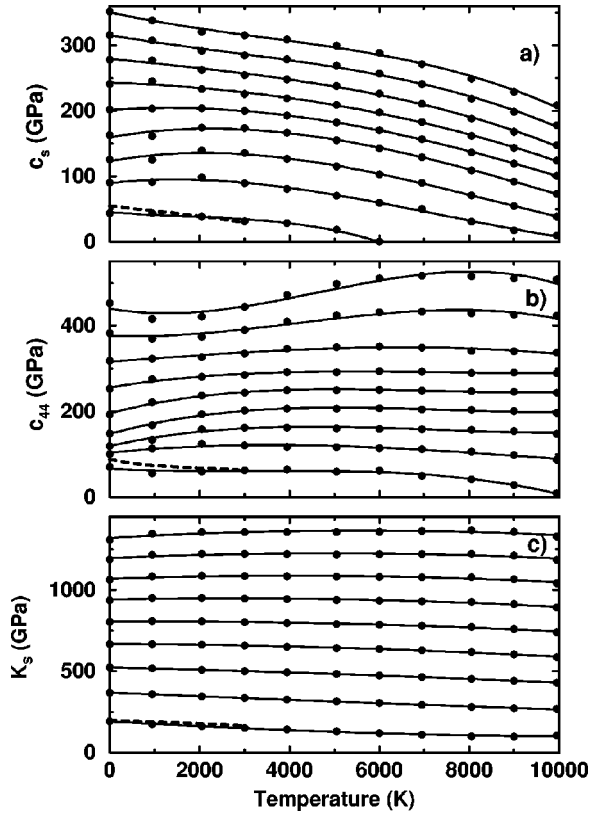


FIG. 2. The elastic constants of bcc Ta as a function of temperature at different pressure from 0 GPa (lowest curve) to 400 GPa (uppermost curve) with 50 GPa interval. (a) shear modulus c_s , (b) shear modulus c_{44} , and (c) adiabatic bulk modulus K_S . Dotted lines are the experimental data from Walker *et al.* (Ref. 28).

thermal elastic constants (c_{ij}^T) are converted to adiabatic constants (c_{ij}^S) according to²⁷

$$c_{ij}^S = c_{ij}^T + \frac{T}{\rho C_V} \lambda_i \lambda_j, \quad (9)$$

where $\lambda_i = \sum_k \alpha_k c_{ik}^T$, α_k is the linear thermal expansion tensor, C_V is the specific heat and ρ is the density. For cubic crystals, Eq. (9) simplifies to

$$c_{11}^S = c_{11}^T + \Delta, \quad (10)$$

$$c_{12}^S = c_{12}^T + \Delta, \quad (11)$$

where

$$\Delta = T(\alpha K_T)^2 / (\rho C_V) = \rho C_V T \gamma^2 = T \alpha K_T \gamma \quad (12)$$

with α is the thermal expansion coefficient, γ is the Grüneisen parameter, and K_T is the isothermal bulk modulus. The thermodynamic parameters were computed self-consistently from the thermal equation of state.⁴ The correction is zero for c_{44} and c_s . Δ increases with temperature but decreases with pressure; at 3000 K it decreases from 5 to 1% for pressures 50 to 400 GPa for bulk modulus K_T , and at 10 000 K Δ is 29 and 3% for the same pressures.

The shear moduli c_s and c_{44} and adiabatic bulk modulus K_S agree well with the ultrasonic experimental data²⁸ up to 3000 K at zero pressure (Fig. 2). We find that all three moduli are primarily functions of volume, and thermal effects at constant volume are quite small except at the highest pressures. There is some softening of c_s with increasing temperature for all pressures. c_{44} shows a slight softening at the zero pressure with increasing temperature, but they are rather flat for other pressures except for very high pressures. The adiabatic bulk modulus K_S also softens slightly with temperature at low pressures but becomes flat with increasing pressure.

The anisotropy ratio $A = c_{44}/c_s$ is presented as a function of temperature for various pressures at Fig. 3. A increases with increasing temperature at all pressures, but less drastically at high pressures. At lower pressures, this increase is divergent after certain temperature, since the softening of c_s is large enough and it approaches zero. The reversal of the slope of A with pressure shifts to higher pressures with increasing temperature due to thermal expansivity, and occurs at a fixed volume.

Sound velocities are related to the elastic constants by the Christoffel equation²⁹

$$(c_{ijkl} n_j n_k - \rho v^2 \delta_{ij}) u_i = 0, \quad (13)$$

where c_{ijkl} is the elastic constants tensor, \vec{n} is the propagation direction, \vec{u} is the polarization vector, and v is the velocity. Our elastic constants are those appropriate for the equations of motion under hydrostatic reference stress.⁷ For [110] wave propagation direction in a cubic lattice, the longitudinal mode is

$$\rho v^2 = (c_{11} + c_{12} + 2c_{44})/2 \quad (14)$$

TABLE II. The elastic constants for bcc tantalum at various temperatures. All elastic constants units are GPa.

T (K)	c_s	c_{44}	c_{11}^T	c_{11}^S	c_{12}^T	c_{12}^S	K_T	K_S
0	44.05	70.26	249.68	249.68	161.59	161.59	190.95	190.95
947	43.58	56.24	221.71	233.41	134.55	146.27	163.61	175.33
2053	38.61	59.39	189.66	211.95	112.44	134.72	138.18	160.46
3000	31.57	62.48	162.55	192.74	99.41	129.60	120.46	150.65
3947	28.72	64.47	142.15	179.77	84.70	122.32	103.85	141.47
5052	18.34	59.70	107.55	154.15	70.87	117.47	83.10	129.70
6000	0.31	62.05	64.91	120.03	64.29	119.40	64.50	119.61

and two transverse modes are

$$\rho v^2 = c_{44} \quad (15)$$

and

$$\rho v^2 = (c_{11} - c_{12})/2 = c_s \quad (16)$$

polarized along [001] and [1 $\bar{1}$ 0] directions, respectively. For polycrystalline sample, the average isotropic shear modulus G can be determined from single crystal elastic constants according to the Voigt-Reuss-Hill scheme,³⁰ and the isotropically averaged aggregate velocities are given by

$$v_P = [(K + 4/3G)/\rho]^{1/2}, \quad (17)$$

$$v_S = (G/\rho)^{1/2}, \quad (18)$$

$$v_B = (K/\rho)^{1/2}, \quad (19)$$

where v_P , v_S , and v_B are the compressional, shear, and bulk sound velocities. The sound velocities of Ta along the Hugoniot calculated from elastic constants are shown in Fig. 4,

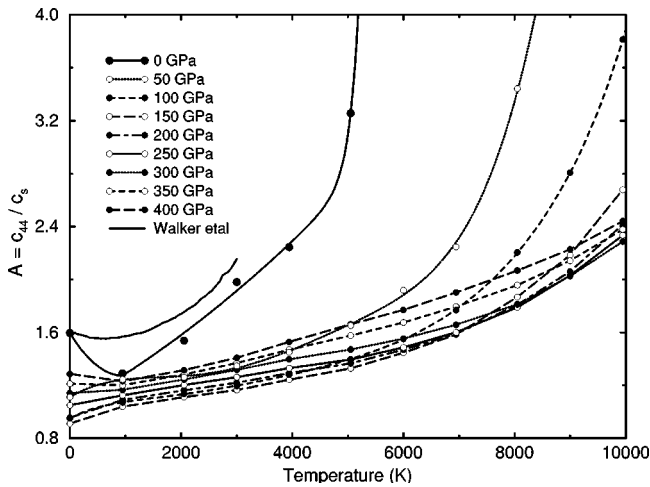


FIG. 3. The anisotropy ratio of elastic constants of Ta as a function of temperature at different pressures from 0 to 400 GPa with 50 GPa interval.

and are compared with the shock sound velocity data from Brown *et al.*³¹ As seen in Fig. 4, there is excellent agreement with shock data. The calculated compressional velocity v_P agrees very well with experimental data up to 200 GPa, and then after 300 GPa the bulk velocity v_B matches the data well. This is because the shocked solid melts around 300 GPa, so the liquid velocity might be represented by V_B . The deviation between 200 and 300 GPa is probably due to pre-melting effects.

In conclusion, the elasticity of bcc Ta is investigated from first principles for pressures up to 400 GPa and temperatures up to 10 000 K. The calculated static elastic constants are in good agreement with available ultrasonic and SAX experimental data. The shear modulus c_{44} and the anisotropy ratio A change behavior with increasing pressure around 150 GPa. Although, the shear modulus c_s softens with increasing temperature at all pressures, c_{44} and K_S soften with temperature at low pressures but then they are rather flat at higher pressures. The main effect of temperature for the thermoelasticity

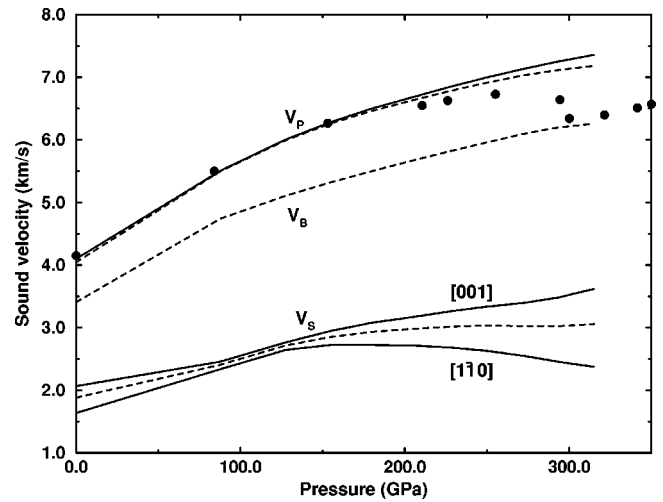


FIG. 4. Sound velocities of Ta along the Hugoniot calculated from elastic constants. Solid lines are the longitudinal and two transverse sound velocities in the [110] direction from single crystal elastic constants. The polarization of the shear waves are given in brackets. The isotropic aggregate velocities are shown by dashed lines. v_P , v_B , and v_S are the compressional, bulk, and shear sound velocities. Filled dots are the shock data from Brown and Shaner (Ref. 31).

of Ta is due to thermal expansivity. The calculated sound velocities along the Hugoniot shows an excellent agreement with shock-wave experimental data.

We thank G. Steinle-Neumann, L. Stixrude, and E. Wasserman for helpful discussions. This work was supported

by DOE ASCI/ASAP Subcontract No. B341492 to Caltech DOE Grant No. W-7405-ENG-48. Computations were performed on the Cray SV1 at the Geophysical Laboratory, supported by NSF Grant No. EAR-9975753 and the W. M. Keck Foundation.

-
- ¹H. Cynn and C.S. Yoo, Phys. Rev. B **59**, 8526 (1999).
²A.C. Mitchell and W.J. Nellis, J. Appl. Phys. **52**, 3363 (1981).
³P. Söderlind and J.A. Moriarty, Phys. Rev. B **57**, 10 340 (1998).
⁴R.E. Cohen and O. Gülseren, Phys. Rev. B **63**, 224101 (2001).
⁵P. Vinet, J. Ferrante, J.R. Smith, and J.H. Rose, J. Phys. C **19**, L467 (1986); P. Vinet, J.H. Rose, J. Ferrante, and J.R. Smith, J. Phys.: Condens. Matter **1**, 1941 (1987).
⁶R.E. Cohen, O. Gülseren, and R.J. Hemley, Am. Mineral. **85**, 338 (2000).
⁷T.H.K. Barron and M.L. Klein, Proc. Phys. Soc. London **85**, 523 (1965).
⁸G. Steinle-Neumann, L. Stixrude, R.E. Cohen, and O. Gülseren, Nature (London) **413**, 57 (2001).
⁹E. Wasserman, L. Stixrude, and R.E. Cohen, Phys. Rev. B **53**, 8296 (1996).
¹⁰D. Alfe, G.D. Price, and M.J. Gillan, Phys. Rev. B **64**, 045123 (2001).
¹¹N.D. Mermin, Phys. Rev. **137**, A1441 (1965).
¹²S.H. Wei and H. Krakauer, Phys. Rev. Lett. **55**, 1200 (1985).
¹³D.J. Singh, *Planewaves, Pseudopotentials, and the LAPW Method* (Kluwer Academic, Boston, 1994).
¹⁴J.P. Perdew, K. Burke, and M. Ernzerhof, Phys. Rev. Lett. **77**, 3865 (1996).
¹⁵H.J. Monkhorst and J.D. Pack, Phys. Rev. B **13**, 5188 (1976).
¹⁶A.C. Holt, W.G. Hoover, S.G. Gray, and D.R. Shortle, Physica (Amsterdam) **49**, 61 (1970); F.H. Ree and A.C. Holt, Phys. Rev. B **8**, 826 (1973); K. Westera and E.R. Cowley, *ibid.* **11**, 4008 (1975); E.R. Cowley, J. Gross, Z. Gong, and G.K. Horton, *ibid.* **42**, 3135 (1990).
¹⁷O. Gülseren, D.M. Bird, and S.E. Humphreys, Surf. Sci. **402-404**, 827 (1998).
¹⁸*Handbook of Physical Quantities*, edited by I.S. Grigoriev and E.Z. Meilikhov (CRC Press, New York, 1997).
¹⁹S. Mukherjee, R.E. Cohen, and O. Gülseren, Phys. Rev. B (to be published).
²⁰J.P. Perdew and A. Zunger, Phys. Rev. B **23**, 5048 (1981).
²¹N. Troullier and J.L. Martins, Phys. Rev. B **43**, 1993 (1991).
²²S.G. Louie, S. Froyen, and M.L. Cohen, Phys. Rev. B **26**, 1738 (1982).
²³A. Bansil, Solid State Commun. **16**, 885 (1975); R. Prasad and A. Bansil, Phys. Rev. B **21**, 496 (1980); W.R. Fehlner, S.B. Nickerson, and S.H. Vosko, Solid State Commun. **19**, 83 (1976).
²⁴K.W. Katahara, M.H. Manghnani, and E.S. Fisher, J. Phys. F: Met. Phys. **9**, 773 (1979).
²⁵K.W. Katahara, M.H. Manghnani, and E.S. Fisher, J. Appl. Phys. **47**, 434 (1976).
²⁶H. Cynn and C.S. Yoo (unpublished); H. Cynn and C.S. Yoo, Bull. Am. Phys. Soc. **44**, 1288 (1999).
²⁷G.F. Davies, J. Phys. Chem. Solids **35**, 1513 (1974).
²⁸E. Walker and P. Bujard, Solid State Commun. **34**, 691 (1980).
²⁹E.B. Christoffel, Ann. Mat. Pura Appl. **8**, 193 (1877).
³⁰R.W. Hill, Proc. Phys. Soc., London, Sect. A **65**, 349 (1952).
³¹J.M. Brown and J.W. Shaner, *Shock Waves in Condensed Matter-1983*, edited by J.R. Asay, R.A. Graham, and G.K. Straub (Elsevier, New York, 1984), pp. 91–94.